Editors' Suggestion

# Power-Law Density of States in Organic Solar Cells Revealed by the Open-Circuit Voltage Dependence of the Ideality Factor

Maria Saladina,[1,*] Christopher Wöpke,[1] Clemens Göhler,[1] Ivan Ramirez,[2] Olga Gerdes,[2] Chao Liu,[3,4] Ning Li,[3,4,5] Thomas Heumüller,[3,4] Christoph J. Brabec,[3,4] Karsten Walzer,[2] Martin Pfeiffer,[2] and Carsten Deibel[1,†]

[1]*Institut für Physik, Technische Universität Chemnitz, 09126 Chemnitz, Germany*
[2]*Heliatek GmbH, 01139 Dresden, Germany*
[3]*Institute of Materials for Electronics and Energy Technology (i-MEET), Friedrich-Alexander-Universität Erlangen-Nürnberg, 91054 Erlangen, Germany*
[4]*Helmholtz Institute Erlangen-Nürnberg for Renewable Energy (HI ERN), 91058 Erlangen, Germany*
[5]*State Key Laboratory of Luminescent Materials and Devices, Institute of Polymer Optoelectronic Materials and Devices, School of Materials Science and Engineering, South China University of Technology, 510640 Guangzhou, China*

(Received 13 July 2022; revised 27 February 2023; accepted 13 April 2023; published 9 June 2023)

The density of states (DOS) is fundamentally important for understanding physical processes in organic disordered semiconductors, yet hard to determine experimentally. We evaluated the DOS by considering recombination via tail states and using the temperature and open-circuit voltage ($V_{oc}$) dependence of the ideality factor. By performing Suns-$V_{oc}$ measurements, we find that the energetic disorder increases deeper into the band gap, which is not expected for a Gaussian or exponential DOS. The linear dependence of the disorder on energy reveals the power-law DOS in organic solar cells.

DOI: 10.1103/PhysRevLett.130.236403

The dominant recombination mechanism in a solar cell is intimately related to the ideality factor [1–3]. For inorganic semiconductors, the closer the ideality factor gets to 2, the more dominant the share of trap-assisted recombination [4]. This connection is more complex for organic materials used in the state-of-the-art solar cells due to the energetic disorder inherent to these systems, giving rise to wave function localization. Consequently, charge carrier transport and recombination in these disordered materials strongly depend on the energetic distribution of localized states [5–9]. If the density of states (DOS) can be approximated by a Gaussian, the ideality factor becomes unity and independent of temperature [9,10]. However, temperature-independent ideality factors equal to 1 are yet to be reported for organic donor-acceptor systems [11–14], implying that the DOS is more complicated in these materials [15–17].

In this Letter, we seek to unravel the real shape of the DOS in a set of solar cells based on organic semiconductor blends. To achieve this aim, we determine ideality factors from temperature-dependent Suns-$V_{oc}$ measurements. We connect the results to theoretical predictions by the multiple-trapping-and-release (MTR) model [7,8,18,19], using different combinations of the Gaussian and exponential DOS functions [20–25] to describe the energetic state distribution of electrons and holes. Depending on the shape of the DOS and the dominant recombination mechanism, the temperature dependence of the ideality factor differs [9], which allows us to assign specific recombination models to the investigated systems. We find that the characteristic energy of the DOS distribution in these organic solar cells depends on the energetic position within the DOS, resulting in a power-law distribution of localized states.

Current-voltage characteristics of a solar cell are usually approximated by the diode equation [26]. The recombination rate $R$ enters the diode equation via recombination current density $j_{rec}$, which at the open-circuit conditions takes the form [27]

$$j_{rec} = e\int_0^L R(x)dx \approx eLR = j_0 \exp\left(\frac{eV_{oc}}{n_{id}k_BT}\right). \quad (1)$$

Here $L$ stands for the active layer thickness, $j_0$ is the dark saturation current density, $n_{id}$ is the ideality factor, $V_{oc}$ is the open-circuit voltage, $e$ is the elementary charge, $k_B$ is the Boltzmann constant, and $T$ is the temperature. To determine the DOS, we evaluate the dependence of $n_{id}$ on $R$.

In organic disordered materials, the localized states in the DOS that lie below the transport energy act as traps, which capture mobile charge carriers [28]. Trapped charge carriers can be thermally released and contribute to photoconductivity. During this process of multiple trapping and release [7,8,18,19], some share of charge carriers recombines and is lost to the photocurrent. In the MTR model, the

 

fraction of the mobile charge carrier density is expressed through parameter $\theta$, the trapping factor, which depends on the DOS distribution [7,19,29]. The density of mobile and trapped charge carriers is expressed as $n_c = \theta n$ and $n_t = (1-\theta)n$, respectively, with $\theta \leq 1$. As the density of trapping states is much larger than the charge carrier density, most relaxed charge carriers populate energy sites in the DOS tail [30]. Thus, $n_c \ll n_t \approx n$ and $\theta \ll 1$, inferring that recombination is mainly trap mediated. Noting that, due to the nature of photogeneration, $n = p$, the recombination rate becomes

$$\begin{aligned} R &\approx k_{r,n} n_c p_t + k_{r,p} n_t p_c \\ &\approx (k_{r,n}\theta_n + k_{r,p}\theta_p) n^2. \end{aligned} \tag{2}$$

Here $k_r$ stands for the recombination prefactor, and the subscript denotes which of the charge carriers, electrons $n$ or holes $p$, are mobile. The finite escape probability from the charge-transfer state back to the separated state, if present, is included in $k_r$ and reduces it compared to the Langevin prefactor $k_L = e(\mu_n + \mu_p)/\varepsilon$ [31–33]. Additionally, $k_r$ contains the effect of active layer morphology that causes its further deviation from $k_L$ [34–37].

The two recombination channels in Eq. (2) are distinguished by the type of mobile charge carrier. One of the channels is dominant if its recombination prefactor and/or its trapping factor is larger than for the other channel. Thus, the exact expression of $R$ depends on (i) the physical parameters, e.g., mobility, of the mobile charge carrier type through the recombination prefactor $k_r$, (ii) the DOS of this charge carrier type through the trapping factor $\theta$, and (iii) the DOS of both charge carriers involved in the dominant recombination channel through the total charge carrier concentration $n$.

To determine and evaluate $n_{\mathrm{id}}$, we focus on the most prevalent models used to approximate the DOS distributions in organic semiconductors—the Gaussian and exponential DOS [20–25]. The depth of trap states depends on the characteristic energy, i.e., the disorder parameter $\sigma$ and the Urbach energy $E_U$, respectively. The resulting form of Eq. (2) is defined by four combinations of these DOS distributions [see Supplemental Material Eqs. (S11)–(S14) [38] ]. For the detailed derivation, the interested reader is referred to the comprehensive work of Hofacker and Neher [9]. Here, we build on a mere fraction of their results related to the ideality factor and summarize relevant parts of the derivation in the Supplemental Material [38]. The ideality factor is obtained by comparing Eq. (1) to the equations of $R$ for the DOS combinations discussed above.

Without loss of generality, we describe the dominant recombination channel involving mobile holes recombining with trapped electrons. The trapped electrons in the recombination channel ($n_t \approx n$) control the temperature dependence of the ideality factor, while the mobile holes ($p_c = \theta_p p$) control the recombination order. If the DOS of electrons is described by a Gaussian, in the low concentration limit we arrive at $n_{\mathrm{id}} = 1$, independent of temperature [9,10,40]. This is true irrespective of whether mobile holes come from the Gaussian or exponential DOS. An ideality factor of unity, however, is not observed experimentally in organic semiconductors [11–14].

In contrast, if the DOS of trapped electrons is exponential, the ideality factor is temperature dependent. When such electrons recombine with mobile holes from a Gaussian DOS, the ideality factor is independent of $\sigma$ and is expressed as [9]

$$n_{\mathrm{id}} = \frac{E_U + k_B T}{2 k_B T}. \tag{3}$$

If mobile holes are also represented by an exponential DOS, the ideality factor is given by [9,12,41,42]

$$n_{\mathrm{id}} = \frac{2E_U}{E_U + k_B T}. \tag{4}$$

We refer to these models as the "mixed DOS" and "exponential DOS," respectively. In order to shed light on the shape of the DOS in organic materials, our focus lies on the temperature dependence of the ideality factor, with the models underlying Eqs. (3) and (4) as the starting point.

To verify that the DOS can be established through ideality factors, we chose the well-studied hydrogenated amorphous silicon solar cell as a reference due to its exponential DOS. We then expanded our investigation to a set of material systems representative of typical organic solar cell classes, such as solution-processed fullerene (P3HT:$PC_{61}BM$) and nonfullerene acceptor devices (PM6:Y6), along with thermally evaporated small-molecule solar cells (DCV-V-Fu-Ind-Fu-V:$C_{60}$). The details of molecular structure and device fabrication are given in the Supplemental Material [38].

We employ illumination intensity-dependent $V_{\mathrm{oc}}$ measurements to determine ideality factors in the absence of series and transport resistance [43–45]. Figure 1(a) shows the Suns-$V_{\mathrm{oc}}$ data of an a-Si:H solar cell between 150 and 300 K. The regions of low light intensity are influenced by low shunt resistance. Roughly above 1 sun, $V_{\mathrm{oc}}$ becomes limited by the contacts, which is more pronounced at low temperatures. Ideality factors were extracted from the slope of $\Phi(V_{\mathrm{oc}})$ according to [13]

$$n_{\mathrm{id}} = \frac{e}{k_B T}\left(\frac{d\ln\Phi}{dV_{\mathrm{oc}}}\right)^{-1}. \tag{5}$$

For each temperature, the data can be fitted with a single slope over 2 orders of magnitude of light intensities.

We show the resulting ideality factors as a function of the inverse temperature in Fig. 1(b). Consistent with van Berkel *et al.* [41], we observe the decrease of $n_{\mathrm{id}}$ of the a-Si:H solar

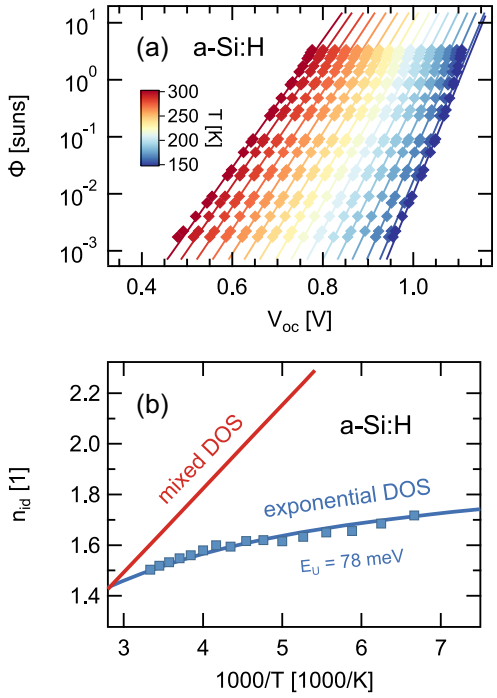


FIG. 1. (a) Suns-$V_{oc}$ data (symbols) of a-Si:H solar cell fitted with Eq. (5) (solid lines). (b) Temperature-dependent ideality factor $n_{id}$ extracted from the fits in comparison to Eqs. (3) and (4).

cell with higher temperature from 1.7 at 150 K to 1.5 at 300 K. The temperature dependence of $n_{id}$ can be fitted with Eq. (4) and therefore is assigned to the trap-assisted recombination of charge carriers within the exponential density of states. The fit yields the Urbach energy of ≈78 meV, in agreement with the literature [41,46], which is independent of temperature and light intensity. In the exponential DOS model $n_{id} \propto (E_U + k_B T)^{-1}$, resulting in a sublinear dependence on $1/T$. A mixed DOS would lead to a distinctly different temperature dependence of the ideality factor, as $n_{id} \propto 1/T$ according to Eq. (3).

We now extend the scope of the study to organic donor-acceptor systems. Figure 2 shows ideality factors of P3HT:$PC_{61}BM$, PM6:Y6, and DCV-V-Fu-Ind-Fu-V:$C_{60}$. First, we note that, at each temperature, $n_{id}$ has several values corresponding to the local slope of $\Phi(V_{oc})$. Hence, in contrast to a-Si:H, the ideality factor of the organic systems we investigate here is light intensity dependent and generally decreases with increasing light intensity. Initially, it seems problematic to assign a specific recombination model based on the temperature dependence of $n_{id}$ at a certain illumination intensity (cf. Supplemental Material Fig. S05 [38]). The position within the DOS depends on both temperature and illumination intensity. For a fixed range of illumination intensities, at lower temperatures we probe states closer to the effective band gap, as compared to higher temperatures. If the DOS of trapped charge carriers is not strictly exponential, its characteristic energy changes with the quasi-Fermi level splitting (QFLS), something not accounted for by the method.

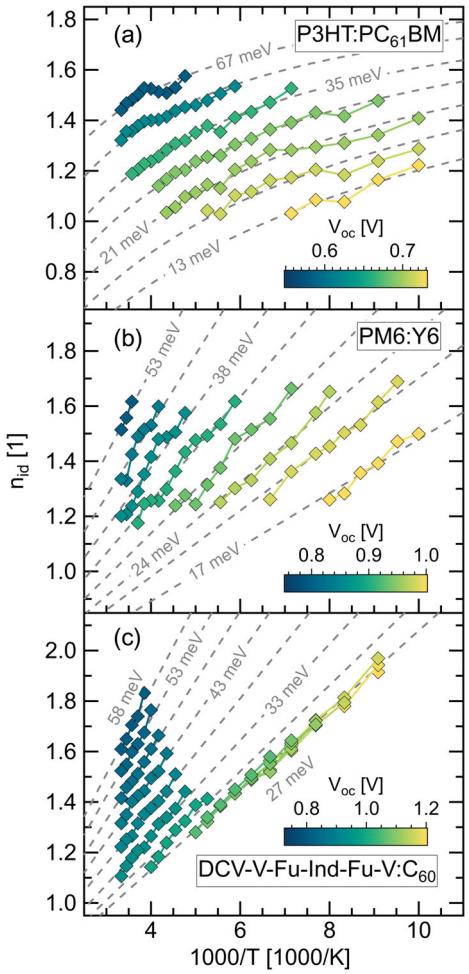


FIG. 2. Temperature-dependent ideality factors $n_{id}$ of (a) P3HT:$PC_{61}BM$, (b) PM6:Y6, and (c) DCV-V-Fu-Ind-Fu-V:$C_{60}$ (symbols). Darker color corresponds to lower $V_{oc}$, i.e., deeper subgap energy states. Dashed lines are the calculated $n_{id}(E_U, T)$ according to Eq. (4) for P3HT:$PC_{61}BM$ and Eq. (3) for PM6:Y6 and DCV-V-Fu-Ind-Fu-V:$C_{60}$. $E_U$ increases with the DOS depth for all three systems.

Instead, we evaluate the data at fixed $V_{oc}$ (cf. Fig. S06 [38]). The QFLS, approximated by $V_{oc}$, samples the combined DOS of electrons and holes at a certain energy. The Urbach energy, which is a measure of disorder for the exponential DOS distribution, is independent of temperature at fixed $V_{oc}$, and the ideality factor describes the dominant recombination mechanism at this DOS depth. Coming back to Fig. 2, we see our approach paying off. For a given $V_{oc}$, the relation between $n_{id}$ and $1/T$ can be assigned to specific recombination models for all three material systems. Ideality factors of P3HT:$PC_{61}BM$ in Fig. 2(a) at a given $V_{oc}$ follow the exponential DOS model (4), similar to what we found for a-Si:H earlier. PM6:Y6 and DCV-V-Fu-Ind-Fu-V:$C_{60}$ in Figs. 2(b) and 2(c), on the other hand, are best described by the mixed DOS model (3).

We calculate $n_{id}$ using different values of $E_U$ (indicated by dashed lines in the figure) and find good agreement with

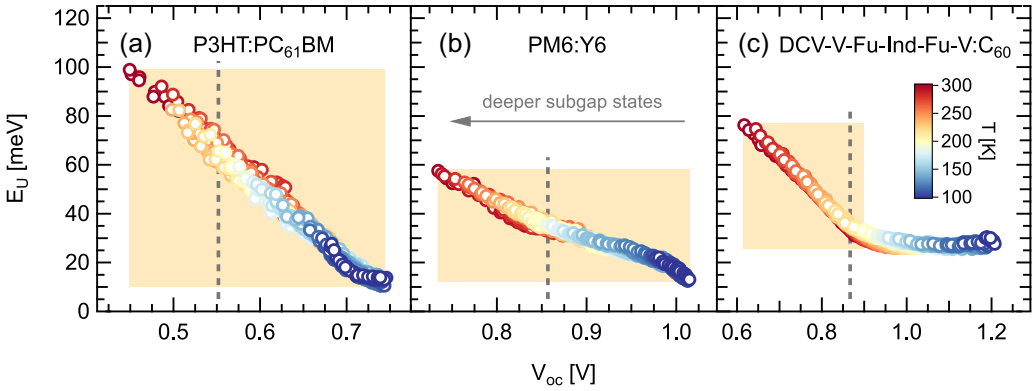


FIG. 3. Urbach energies $E_U$ as a function of the quasi-Fermi level splitting, approximated by $V_{oc}$. $E_U$ was calculated from $n_{id}(T)$ according to Eq. (4) for (a) P3HT:$PC_{61}$BM and Eq. (3) for (b) PM6:Y6 and (c) DCV-V-Fu-Ind-Fu-V:$C_{60}$. $E_U$ is independent of $T$, while it depends linearly on $V_{oc}$ within the highlighted areas, inferring that the DOS is described by a power law. Roughly constant $E_U$ outside of the highlighted area is an indication of the exponential DOS. Dashed lines correspond to $V_{oc}$ at 1 sun illumination intensity at room temperature.

the data. For a strictly exponential DOS, the Urbach energy is constant and describes the DOS globally. For all three organic donor-acceptor systems, however, the Urbach energy describes the DOS of trapped charge carriers only locally and becomes a function of energy, inferring that the exponential DOS acts as a local approximation of the real DOS at a given QFLS [16]. The deeper we are probing in the density of states, the larger the $E_U$. The DOS of the thermally evaporated DCV-V-Fu-Ind-Fu-V:$C_{60}$ solar cell is nearly exponential above 0.90 V, as $E_U$ is roughly constant in this region.

Figure 3 shows the relation between the Urbach energy and the QFLS. First, we note a striking convergence of $E_U$ at different temperatures for all the systems, strengthening our confidence in the analytical approach and the assigned system-specific recombination models. $E_U$ depends linearly on the QFLS in the regions of nonconstant Urbach energy (highlighted areas in the figure). This linearity helps to unravel the real shape of the density of states. For the exponential DOS $g_{exp}(E)$,

$$\frac{d \ln g_{exp}(E)}{dE} = \frac{1}{E_U}. \tag{6}$$

We emphasize again that in our case the exponential function acts as a local approximation of the real DOS. With the linear relation that we observe, $E_U(E) = (E - E_0)/\xi$, the derivative of the real DOS distribution is given by

$$\frac{d \ln g(E)}{dE} = \frac{\xi}{E - E_0}. \tag{7}$$

This relation leads to $\ln g(E) \propto \xi \ln (E - E_0)$, and the ultimate form of the DOS distribution is a power law,

$$g(E) \propto (E - E_0)^{\xi}. \tag{8}$$

To our knowledge, the power-law density of states has not been reported for organic solar cells before. However, it must be considered when explaining experimental data and simulating the physics of organic semiconductors, as we observe this DOS distribution in all the donor-acceptor systems investigated herein. The power-law DOS can be assigned to P3HT:$PC_{61}$BM and PM6:Y6 in the whole measured data range. The density of states of DCV-V-Fu-Ind-Fu-V:$C_{60}$ follows the power law up to ca. 0.90 V and changes its shape to exponential at higher $V_{oc}$. Compared to an exponential DOS, the power law is described by a narrower tail. Hence, there are fewer available states for the charge carriers to fill up, resulting in a higher $V_{oc}$ than would be expected for the exponential DOS. By averaging, we find that under 1 sun illumination at room temperature $E_U \approx 66$ meV for P3HT:$PC_{61}$BM, similar to previous reports [12,42,47]. In DCV-V-Fu-Ind-Fu-V:$C_{60}$ and PM6:Y6, the energetic disorder is reduced ($E_U \approx 35$ meV) [48–50], and the trap distribution is narrower compared to P3HT:$PC_{61}$BM. Lower disorder is, in general, beneficial to the solar cell performance, as it leads to enhanced charge carrier transport and reduced $V_{oc}$ losses [51–53].

In conclusion, we employ temperature and illumination intensity-dependent $V_{oc}$ measurements to determine the type of the density of states in PM6:Y6, DCV-V-Fu-Ind-Fu-V:$C_{60}$, and P3HT:$PC_{61}$BM organic solar cells. We find that the temperature dependence of the ideality factor can be explained in the framework of the multiple-trapping-and-release model, but only if analyzed at a given open-circuit voltage. For all the investigated organic systems, the density of states of trapped charge carriers participating in recombination is locally approximated by the exponential one, where the characteristic energy of the distribution decreases linearly with increasing quasi-Fermi level splitting. Our results establish that the density of states

in these solar cells follows a power law, which has not been reported for organic donor-acceptor systems up to date. We suggest that the temperature-dependent experiments designed to understand recombination mechanisms in these disordered systems have to be conducted at the same quasi-Fermi level splitting to ensure correct interpretation of the results.

The authors are grateful to J. Gorenflot, KAUST, for his valuable comments on the Letter. We thank the Deutsche Forschungsgemeinschaft (DFG) for funding this work (Research Unit FOR 5387 POPULAR, Project No. 461909888).

*maria.saladina@physik.tu-chemnitz.de
†deibel@physik.tu-chemnitz.de

[1] G. A. H. Wetzelaer, M. Kuik, H. T. Nicolai, and P. W. M. Blom, Phys. Rev. B **83**, 165204 (2011).
[2] C. Göhler, A. Wagenpfahl, and C. Deibel, Adv. Electron. Mater. **4**, 1700505 (2018).
[3] W. Tress, M. Yavari, K. Domanski, P. Yadav, B. Niesen, J. P. C. Baena, A. Hagfeldt, and M. Graetzel, Energy Environ. Sci. **11**, 151 (2018).
[4] C.-T. Sah, R. N. Noyce, and W. Shockley, Proc. IRE **45**, 1228 (1957).
[5] H. Bässler, Phys. Status Solidi (b) **175**, 15 (1993).
[6] O. Rubel, S. D. Baranovskii, P. Thomas, and S. Yamasaki, Phys. Rev. B **69**, 014206 (2004).
[7] S. Baranovskii, Phys. Status Solidi (b) **251**, 487 (2014).
[8] A. Nenashev, J. Oelerich, and S. Baranovskii, J. Phys. Condens. Matter **27**, 093201 (2015).
[9] A. Hofacker and D. Neher, Phys. Rev. B **96**, 245204 (2017).
[10] J. C. Blakesley and D. Neher, Phys. Rev. B **84**, 075210 (2011).
[11] R. A. Street, A. Krakaris, and S. R. Cowan, Adv. Funct. Mater. **22**, 4608 (2012).
[12] A. Foertig, J. Rauh, V. Dyakonov, and C. Deibel, Phys. Rev. B **86**, 115302 (2012).
[13] K. Tvingstedt and C. Deibel, Adv. Energy Mater. **6**, 1502230 (2016).
[14] L. Perdigón-Toro, L. Q. Phuong, F. Eller, G. Freychet, E. Saglamkaya, J. I. Khan, Q. Wei, S. Zeiske, D. Kroh, S. Wedler, A. Köhler, A. Armin, F. Laquai, E. M. Herzig, Y. Zou, S. Shoaee, and D. Neher, Adv. Energy Mater. **12**, 2103422 (2022).
[15] R. C. MacKenzie, T. Kirchartz, G. F. Dibb, and J. Nelson, J. Phys. Chem. C **115**, 9806 (2011).
[16] R. C. MacKenzie, C. G. Shuttle, M. L. Chabinyc, and J. Nelson, Adv. Energy Mater. **2**, 662 (2012).
[17] J. O. Oelerich, D. Huemmer, and S. D. Baranovskii, Phys. Rev. Lett. **108**, 226403 (2012).
[18] J. Noolandi, Phys. Rev. B **16**, 4466 (1977).
[19] V. Arkhipov, V. Kolesnikov, and A. Rudenko, J. Phys. D **17**, 1241 (1984).
[20] P. Mark and W. Helfrich, J. Appl. Phys. **33**, 205 (1962).
[21] G. Paasch and S. Scheinert, J. Appl. Phys. **107**, 104501 (2010).
[22] G. Garcia-Belmonte, Sol. Energy Mater. Sol. Cells **94**, 2166 (2010).
[23] T. Kirchartz and J. Nelson, Phys. Rev. B **86**, 165201 (2012).
[24] T. M. Burke, S. Sweetnam, K. Vandewal, and M. D. McGehee, Adv. Energy Mater. **5**, 1500123 (2015).
[25] B. Xiao, P. Calado, R. C. I. MacKenzie, T. Kirchartz, J. Yan, and J. Nelson, Phys. Rev. Appl. **14**, 024034 (2020).
[26] W. Shockley, Bell Syst. Tech. J. **28**, 435 (1949).
[27] U. Würfel, D. Neher, A. Spies, and S. Albrecht, Nat. Commun. **6**, 6951 (2015).
[28] V. I. Arkhipov, E. V. Emelianova, and G. J. Adriaenssens, Phys. Rev. B **64**, 125125 (2001).
[29] G. J. Adriaenssens, S. D. Baranovskii, W. Fuhs, J. Jansen, and Ö. Öktü, Phys. Rev. B **51**, 9661 (1995).
[30] V. Arkhipov, I. Fishchuk, A. Kadashchuk, and H. Bässler, Charge transport in disordered organic semiconductors, in *Photophysics of Molecular Materials: From Single Molecules To Single Crystals* (Wiley-VCH Verlag, Weinheim, 2006), Chap. 6, pp. 261–366, 10.1002/3527607323.ch6.
[31] P. Langevin, Ann. Chim. Phys. **28**, 433 (1903).
[32] C. L. Braun, J. Chem. Phys. **80**, 4157 (1984).
[33] S. Shoaee, A. Armin, M. Stolterfoht, S. M. Hosseini, J. Kurpiers, and D. Neher, Solar RRL **3**, 1900184 (2019).
[34] L. Koster, V. Mihailetchi, and P. Blom, Appl. Phys. Lett. **88**, 052104 (2006).
[35] J. Gorenflot, M. C. Heiber, A. Baumann, J. Lorrmann, M. Gunz, A. Kämpgen, V. Dyakonov, and C. Deibel, J. Appl. Phys. **115**, 144502 (2014).
[36] M. C. Heiber, C. Baumbach, V. Dyakonov, and C. Deibel, Phys. Rev. Lett. **114**, 136602 (2015).
[37] M. C. Heiber, T.-Q. Nguyen, and C. Deibel, Phys. Rev. B **93**, 205204 (2016).
[38] See Supplemental Material at http://link.aps.org/supplemental/10.1103/PhysRevLett.130.236403 for experimental methods, details of the theoretical model, and data analysis, which includes Ref. [39].
[39] R. Fitzner, E. Mena-Osteritz, A. Mishra, G. Schulz, E. Reinold, M. Weil, C. Körner, H. Ziehlke, C. Elschner, K. Leo, M. Riede, M. Pfeiffer, C. Uhrich, and P. Bäuerle, J. Am. Chem. Soc. **134**, 11064 (2012).
[40] W. F. Pasveer, J. Cottaar, C. Tanase, R. Coehoorn, P. A. Bobbert, P. W. M. Blom, D. M. de Leeuw, and M. A. J. Michels, Phys. Rev. Lett. **94**, 206601 (2005).
[41] C. van Berkel, M. Powell, A. Franklin, and I. French, J. Appl. Phys. **73**, 5264 (1993).
[42] T. Kirchartz, B. E. Pieters, J. Kirkpatrick, U. Rau, and J. Nelson, Phys. Rev. B **83**, 115209 (2011).
[43] M. Wolf and H. Rauschenbach, Adv. Energ. Convers. **3**, 455 (1963).
[44] T. Kirchartz, F. Deledalle, P. S. Tuladhar, J. R. Durrant, and J. Nelson, J. Phys. Chem. Lett. **4**, 2371 (2013).
[45] C. Wöpke *et al.*, Nat. Commun. **13**, 3786 (2022).
[46] R. Wehrspohn, S. Deane, I. French, I. Gale, J. Hewett, M. Powell, and J. Robertson, J. Appl. Phys. **87**, 144 (2000).
[47] B. Jarzkąbek, P. Nitschke, B. Hajduk, M. Domański, and H. Bednarski, Polymer Test. **88**, 106573 (2020).
[48] A. Karki, J. Vollbrecht, A. L. Dixon, N. Schopp, M. Schrock, G. M. Reddy, and T.-Q. Nguyen, Adv. Mater. **31**, 1903868 (2019).

[49] J. Wu, J. Lee, Y.-C. Chin, H. Yao, H. Cha, J. Luke, J. Hou, J.-S. Kim, and J. R. Durrant, Energy Environ. Sci. **13**, 2422 (2020).
[50] T. Yang, R. Ma, H. Cheng, Y. Xiao, Z. Luo, Y. Chen, S. Luo, T. Liu, X. Lu, and H. Yan, J. Mater. Chem. A **8**, 17706 (2020).
[51] I. Lange, J. Kniepert, P. Pingel, I. Dumsch, S. Allard, S. Janietz, U. Scherf, and D. Neher, J. Phys. Chem. Lett. **4**, 3865 (2013).
[52] S. D. Collins, C. M. Proctor, N. A. Ran, and T.-Q. Nguyen, Adv. Energy Mater. **6**, 1501721 (2016).
[53] C. Göhler and C. Deibel, ACS Energy Lett. **7**, 2156 (2022).

Supplemental material

# Power-law density of states in organic solar cells revealed by the open-circuit voltage dependence of the ideality factor

Maria Saladina,[1] Christopher Wöpke,[1] Clemens Göhler,[1] Ivan Ramirez,[2] Olga Gerdes,[2] Chao Liu,[3,4] Ning Li,[3,4,5] Thomas Heumüller,[3,4] Christoph J. Brabec,[3,4] Karsten Walzer,[2] Martin Pfeiffer,[2] and Carsten Deibel[1]

[1] *Institut für Physik, Technische Universität Chemnitz, 09126 Chemnitz, Germany*
[2] *Heliatek GmbH, 01139 Dresden, Germany*
[3] *Institute of Materials for Electronics and Energy Technology (i-MEET), Friedrich-Alexander-Universität Erlangen-Nürnberg, 91054 Erlangen, Germany*
[4] *Helmholtz Institute Erlangen-Nürnberg for Renewable Energy (HI ERN), 91058 Erlangen, Germany*
[5] *State Key Laboratory of Luminescent Materials and Devices, Institute of Polymer Optoelectronic Materials and Devices, School of Materials Science and Engineering, South China University of Technology, 510640 Guangzhou, China*

## S1. EXPERIMENTAL METHODS

### A. Materials

**DCV-V-Fu-Ind-Fu-V:$C_{60}$**. DCV-V-Fu-Ind-Fu-V is a proprietary, oligomeric absorber material of Heliatek GmbH as shown in Figure S01. It belongs to the the class of A-D-A (acceptor - donor - acceptor) type molecules, similar to the well-known DCV-oligothiophenes like DCV5T[1]. A mixture with fullerene $C_{60}$ is easily achieved by thermal co-evaporation in ultrahigh vacuum.

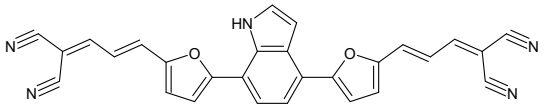


**Figure S01.** Molecular structure of DCV-V-Fu-Ind-Fu-V.

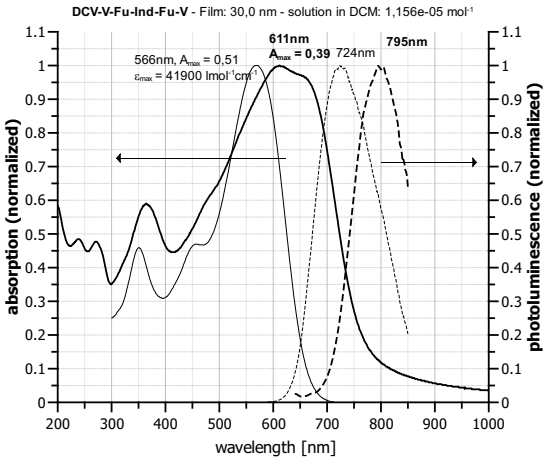


**Figure S02.** Optical characteristics of DCV-V-Fu-Ind-Fu-V in a 30 nm thick film (bold lines) and in dicyanomethane solution (thin lines). Solid lines refer to absorption, dashed lines represent photoluminescence data.

### B. Device fabrication

**a-Si:H**. Hydrogenated amorphous silicon solar cell was purchased from Lemo-Solar GmbH.

**P3HT:PC$_{61}$BM**. P3HT and PC$_{61}$BM were purchased from Ossila BV, and used without further purification. The active layer blend solution (1:0.8 w/w, 30 mg ml$^{-1}$ in chlorobenzene) was stirred overnight at 50 °C in the glovebox. A glass substrate with pre-patterned indium tin oxide (ITO) was cleaned in ultrasonic bath with detergent, acetone, isopropanol and deionised water. After exposure to low-pressure oxygen plasma for 5 min, a 35 nm layer of poly(3,4-ethylenedioxythiophene) polystyrene sulfonate (PEDOT:PSS, Clevios AI 4083, Heraeus Deutschland GmbH & Co. KG) was spin-coated and annealed at 140 °C for 10 min. The substrate was transferred to a nitrogen-filled glovebox, where the active layer was spin-coated at 1000 r.p.m. from blend solution and annealed at 150 °C for 10 min. The device was completed by 2 nm of thermally evaporated Ca and 150 nm of Al with a base pressure below $10^{-6}$ mbar through a shadow mask, and had an active area of 4.0 mm$^2$.

**PM6:Y6**. PM6 and Y6 were purchased from 1-Material Inc. and used as received. The active layer blend solution (1:1.2 w/w, 10 mg ml$^{-1}$ in chloroform with 0.5 vol.-% of 1-chloronaphthalene) was stirred overnight at room temperature. ITO-coated glass substrate was cleaned with detergent, acetone, isopropanol and deionised water. A 35 nm thick PEDOT:PSS layer was spin-coated subsequent to a 5 min oxygen plasma treatment, and annealed at 140 °C for 10 min. The active layer was spin-coated from blend solution at 3000 r.p.m. in a nitrogen-filled glovebox. The solar cell was completed by 5 nm of bathocuproine (Ossila BV) and 100 nm of Ag, thermally evaporated through a shadow mask, yielding an active area of 4.0 mm$^2$.

**DCV-V-Fu-Ind-Fu-V:C$_{60}$**. All the layers were deposited through thermal evaporation in an ultra-high vacuum chamber onto a cleaned glass substrate with structured ITO. An electron transport layer consisted of 5 nm of n-doped (20 %) C$_{60}$ and 15 nm of C$_{60}$. The active layer composed of DCV-V-Fu-Ind-Fu-V:C$_{60}$ (2:1 w/w) was co-evaporated onto a 50 °C hot substrate, which was subsequently cooled down for 60 min. After that, the substrate was covered with a hole transport layer consisting of 10 nm of BPAPF (Lumtec, Taiwan) and 20 nm of p-doped (10 %) BPAPF. The solar cell was finished by a 100 nm thick Al electrode, and had an active area of 6.44 mm$^2$. After fabrication, the device was encapsulated under nitrogen atmosphere with a glass lid.

### C. Suns–$V_{oc}$ measurements

Samples were excited by an Omicron LDM A350 continuous wave laser at a wavelength of 515 nm. The illumination intensity was varied by the laser output power and Standa motorised filter wheels with Thorlabs neutral density filters, and monitored by a silicon photodiode throughout the measurement. Open-circuit voltage was measured with a Keithley 2634b source measure unit. During the experiment the sample was held in a Linkam Scientific LTS420 cryostat which maintained low temperature by constant flow of liquid nitrogen using Linkam Scientific LNP96-S liquid nitrogen pump and Linkam Scientific T96-S temperature controller.

## S2. DERIVATION OF THE RECOMBINATION RATE FOR DIFFERENT DOS DISTRIBUTIONS

To make the link between the energetic picture and the ideality factor in the diode equation, the charge carrier density in Eq. (2) is expressed in terms of the effective band gap $E_g$ and the open-circuit voltage $V_{\mathrm{oc}}$. This is achieved by relating the total densities of electrons and holes and then expressing $V_{\mathrm{oc}}$ through the quasi-Fermi level splitting. The resulting expression for the charge carrier concentration $n$, along with the relevant equation for $\theta$, replace the terms in Eq. (2).

### A. Charge carrier statistics

The total charge carrier density in the exponential DOS depends on the characteristic distribution width $E_U$ as[2–6]

$$n_{\mathrm{exp}} = N_0 \cdot \exp\left(\frac{E_F}{E_U}\right), \tag{S1}$$

where $N_0$ stands for the total density of states and $E_F$ is the quasi-Fermi level relative to the transport energy. The transport energy is defined so that the probability of charge carrier release from a trap state with this energy is approaching unity[7]. The trapping factor in the exponential DOS depends on the quasi-Fermi level position and can be related to the charge carrier density in Eq. (S1)[2,5,7]

$$\begin{aligned}\theta_{\mathrm{exp}} &= \exp\left(\frac{E_F}{k_B T}\right) \cdot \exp\left(-\frac{E_F}{E_U}\right) \\ &= N_0^{1-\lambda} \cdot n_{\mathrm{exp}}^{\lambda-1}.\end{aligned} \tag{S2}$$

Here the dispersion parameter $\lambda$ is defined as $\lambda = E_U/k_B T$ with the Boltzmann constant $k_B$ and temperature $T$.

The concentration of charge carriers in the gaussian DOS is given by[3,5,8]

$$n_{\mathrm{gsn}} = N_0 \cdot \exp\left(\frac{\sigma^2}{2(k_B T)^2}\right) \exp\left(\frac{E_F}{k_B T}\right), \tag{S3}$$

where the disorder parameter $\sigma$ also relates the mobile charge carrier density $n_c$ to the total $n$, resulting in the energy-independent trapping factor[3,5,7,9]

$$\theta_{\mathrm{gsn}} = \exp\left(-\frac{\sigma^2}{2(k_B T)^2}\right). \tag{S4}$$

#### 1. *Exponential DOS*

If both charge carrier types occupy exponential DOS, the densities of electrons $n$ and holes $p$ are defined by Eq. (S1). With the relation $n = p$, and, assuming that $E_U$ is the same for electrons and holes, the open-circuit voltage $V_{\mathrm{oc}}$ derived via the quasi-Fermi level splitting $E_F^n - E_F^p$ is

$$\begin{aligned}eV_{\mathrm{oc}} &= E_g + E_U \ln\frac{np}{N_0^2} \\ &= E_g + 2E_U \ln\frac{n}{N_0},\end{aligned} \tag{S5}$$

and the charge carrier density expressed in terms of $V_{\mathrm{oc}}$ and the effective band gap $E_g$ is given by[5,10–12]

$$n = p = N_0 \cdot \exp\left(-\frac{E_g - eV_{\mathrm{oc}}}{2E_U}\right). \tag{S6}$$

### 2. Gaussian DOS

Supposing that the density of states of both electrons and holes is described by a gaussian, the charge carrier density is given by Eq. (S3). Assuming, for simplicity, that $\sigma_n = \sigma_p = \sigma$, and with $n = p$, the open-circuit voltage becomes

$$\begin{aligned} eV_{\mathrm{oc}} &= E_g - \frac{\sigma^2}{k_B T} + k_B T \ln \frac{np}{N_0^2} \\ &= E_g - \frac{\sigma^2}{k_B T} + 2k_B T \ln \frac{n}{N_0}, \end{aligned} \tag{S7}$$

which results in the charge carrier density given by[5,11,13]

$$n = p = N_0 \cdot \exp\left(-\frac{E_g - \sigma^2 (k_B T)^{-1} - eV_{\mathrm{oc}}}{2k_B T}\right). \tag{S8}$$

### 3. Mixed DOS

For the mixed DOS, where the DOS distributions of electrons and holes are different, we assume that electrons are described by the exponential and holes by the gaussian DOS. Their respective densities are defined by Eqs. (S1) and (S3). With equal electron and hole densities $n = p$, the open-circuit voltage $V_{\mathrm{oc}}$ is given by

$$\begin{aligned} eV_{\mathrm{oc}} &= E_g - \frac{\sigma^2}{2k_B T} + E_U \ln \frac{n}{N_0} + k_B T \ln \frac{p}{N_0} \\ &= E_g - \frac{\sigma^2}{2k_B T} + (E_U + k_B T) \ln \frac{n}{N_0}, \end{aligned} \tag{S9}$$

and the charge carrier density is[5]

$$n = p = N_0 \cdot \exp\left(-\frac{E_g - \sigma^2 (2k_B T)^{-1} - eV_{\mathrm{oc}}}{E_U + k_B T}\right). \tag{S10}$$

As seen from Eqs. (S6), (S8) and (S10), different combinations of the electron and hole DOS yield different expressions for the total charge carrier density. These differences in turn lead to different expressions for mobile ($n_c = \theta n$) and trapped ($n_t \approx n$) charge carrier density, and eventually recombination rate, for each case.

## B. The recombination rate

The four combinations of the electron and hole DOS described by the exponential and gaussian distributions are depicted in Figure S03. Following the logical sequence in the main text, the dominant recombination channel is described by recombination of mobile holes with trapped electrons, while not losing any generality. In order to relate the recombination rate $R$ to the effective band gap $E_g$ and the open-circuit voltage $V_{\mathrm{oc}}$, the expressions for $\theta$ and $n$ are used to replace the terms in Eq. (2).

If the density of states of both electrons and holes can be described by the gaussian DOS with the same $\sigma$, we substitute $\theta$ and $n$ in Eq. (2) by Eqs. (S4) and (S8), respectively, and arrive at[5,14]

$$\begin{aligned} R &\approx k_r n^2 \cdot \exp\left(-\frac{\sigma^2}{2(k_B T)^2}\right) \\ &= k_r N_0^2 \cdot \exp\left(-\frac{E_g - \sigma^2 (2k_B T)^{-1} - eV_{\mathrm{oc}}}{k_B T}\right). \end{aligned} \tag{S11}$$

If the dominant recombination channel involves mobile holes from the exponential DOS recombining with all electrons from the gaussian DOS, then the total charge carrier density is given by Eq. (S10) and the trapping factor by Eq. (S2).

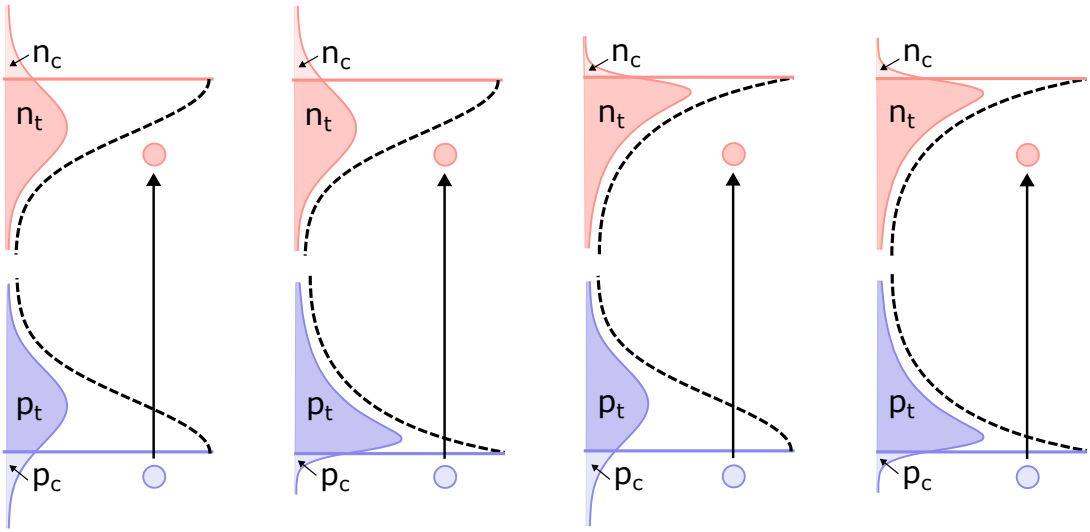


**Figure S03.** Schematics depicting four combinations of the electron and hole densities of states leading to Eqs. (S11) to (S14) (from left to right).

The recombination rate is then expressed as[5]

$$\begin{aligned} R &\approx k_r N_0^{1-\lambda} n^{\lambda+1} \\ &= k_r N_0^2 \cdot \exp\left(-\frac{E_g - \sigma^2 (2k_B T)^{-1} - eV_{\mathrm{oc}}}{k_B T}\right), \end{aligned} \tag{S12}$$

with the same result as for the purely gaussian DOS.

Supposing that the density of states of electrons is described by the exponential, and holes by the gaussian DOS, the total charge carrier concentration given by Eq. (S10) replaces $n$ in Eq. (2). The trapping factor is defined by Eq. (S4), which yields[5]

$$\begin{aligned} R &\approx k_r n^2 \cdot \exp\left(-\frac{\sigma^2}{2(k_B T)^2}\right) \\ &= k_r N_0^2 \cdot \exp\left(-\frac{E_g + \sigma^2 (E_U - k_B T)(2k_B T)^{-2} - eV_{\mathrm{oc}}}{\frac{1}{2}(E_U + k_B T)}\right). \end{aligned} \tag{S13}$$

Finally, for the purely exponential DOS, we use Eqs. (S2) for $\theta$ and (S6) for $n$, which leads to[5,6,10]

$$\begin{aligned} R &\approx k_r N_0^{1-\lambda} n^{\lambda+1} \\ &= k_r N_0^2 \cdot \exp\left[-\frac{E_g - eV_{\mathrm{oc}}}{k_B T}\left(\frac{1}{2} + \frac{k_B T}{2E_U}\right)\right]. \end{aligned} \tag{S14}$$

Comparison of Eq. (1) to the expressions for the recombination rate given by Eqs. (S11) to (S14) yields Eqs. (3) and (4) in the main text.

If the recombination rate $R$ is expressed by Eqs. (S11) or (S12), the ideality factor $n_{\mathrm{id}} = 1$, independent of temperature. Experimental findings, however, suggest that the ideality factor in organic semiconductors differs from unity,[15–18] which leads to two implications. First, in a mixed DOS, the dominant recombination channel involves mobile charge carriers in the gaussian DOS, recombining with trapped charge carriers in the exponential DOS. A gaussian DOS reaches less deep into the band gap so that $\theta$ is generally closer to one than for an exponential DOS. Hence, this channel has a larger share of mobile charge carriers leading, for the same $k_r$, to a larger effective recombination prefactor than for the other channel. Second, the total distribution of localised states is likely more complicated than the gaussian for organic materials.

## S3. DATA ANALYSIS

The ideality factor $n_{\mathrm{id}}$ was calculated from the Suns–$V_{\mathrm{oc}}$ data in Figure S04 using Eq. (5) in the main text

$$n_{\mathrm{id}} = \frac{e}{k_B T} \left( \frac{d \ln \Phi}{d V_{\mathrm{oc}}} \right)^{-1} . \tag{S15}$$

The derivative of $\ln \Phi$ with respect to $V_{\mathrm{oc}}$ was found by taking a second order polynomial fit at each point. The resulting ideality factor values were then interpolated to the same illumination intensity, or open-circuit voltage, for each temperature.

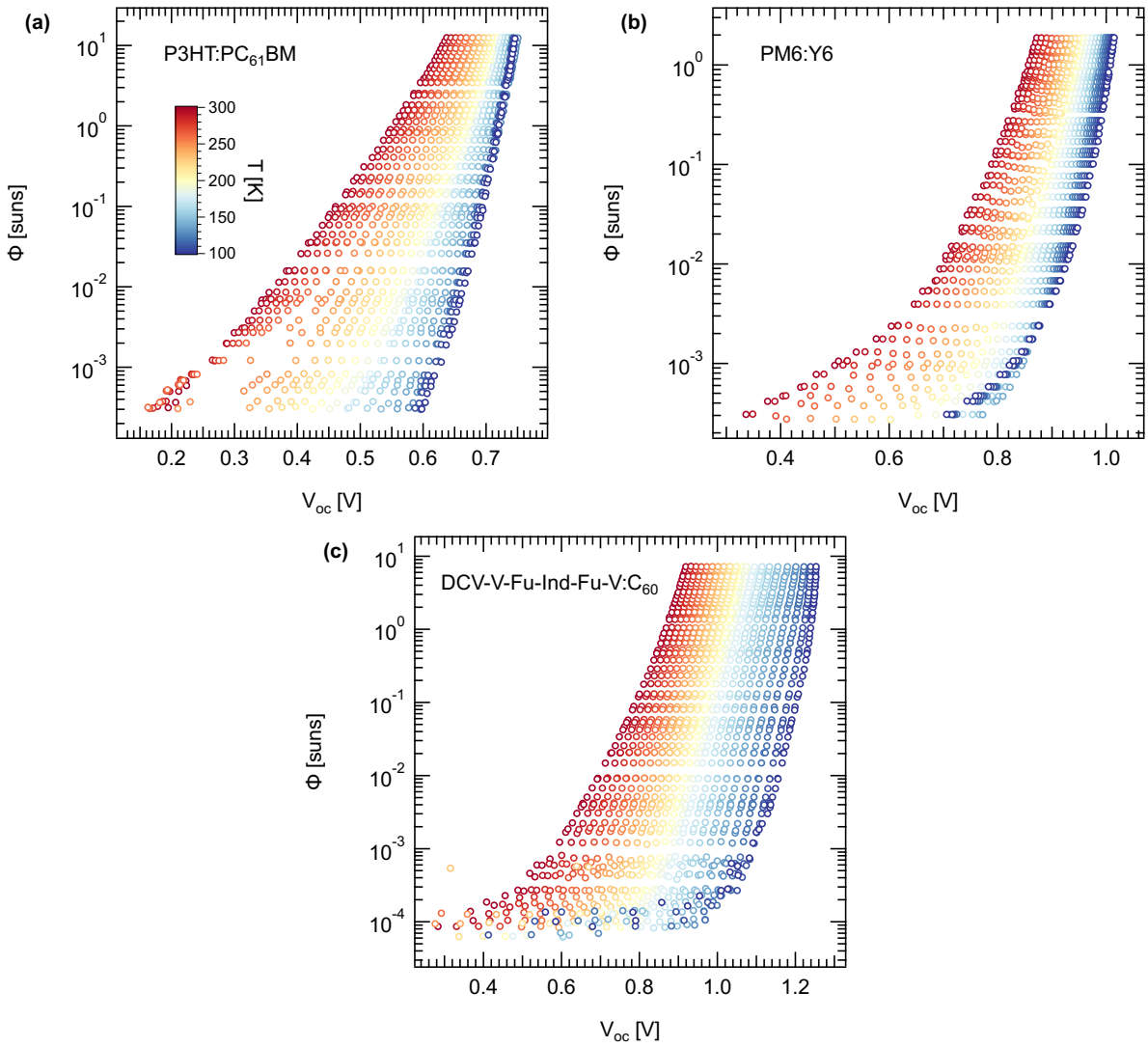


**Figure S04.** Temperature-dependent Suns–$V_{\mathrm{oc}}$ data of (a) P3HT:$PC_{61}BM$, (b) PM6:Y6 and (c) DCV-V-Fu-Ind-Fu-V:$C_{60}$.

**Light intensity-dependent ideality factors**. First, we analyse the temperature dependence of $n_{\mathrm{id}}$ at fixed light intensity. If the DOS of trapped charge carriers in the dominant recombination channel is exponential, the ideality factor is temperature dependent, as we observe in Figure S05. For a given light intensity the quasi-Fermi level splitting increases with lower temperature. $E_U$, the slope of the exponential DOS, is independent of the position within the DOS, therefore $n_{\mathrm{id}}$ is not affected by the temperature dependence of the QFLS. Thus, the light intensity-dependent ideality factor should follow whether the mixed DOS, or the exponential DOS model.

The ideality factor of P3HT:$PC_{61}BM$ at a given light intensity in Figure S05(a) is inversely correlated to $1/T$ between

180 K and 300 K. The recombination models described in the main text, on the other hand, predict whether constant $n_{\mathrm{id}} = 1$ or an increasing $n_{\mathrm{id}}$ with $1/T$. This apparent temperature dependence of $n_{\mathrm{id}}$ at a given light intensity deviates from the models due to the increasing quasi-Fermi splitting at lower temperatures. The same mismatch between the models and the apparent temperature dependence of $n_{\mathrm{id}}$ is observed for DCV-V-Fu-Ind-Fu-V:$C_{60}$ between 240 K and 300 K in Figure S05(c). Only at lower temperatures do the ideality factors of this system converge for different light intensities and follow the mixed DOS recombination model. The temperature dependence of $n_{\mathrm{id}}$ of PM6:Y6 in Figure S05(b) is too weak to be described by the mixed DOS model, and deviates from the exponential DOS model at higher temperatures. At higher illumination intensities the ideality factor approaches unity, but increases substantially at lower light intensities, and therefore can not be assigned to the recombination models characterised by $n_{\mathrm{id}} = 1$. All in all, analysing the temperature dependence of ideality factors at a given light intensity is not an effective strategy to draw conclusions about the dominant recombination mechanism present in a solar cell.

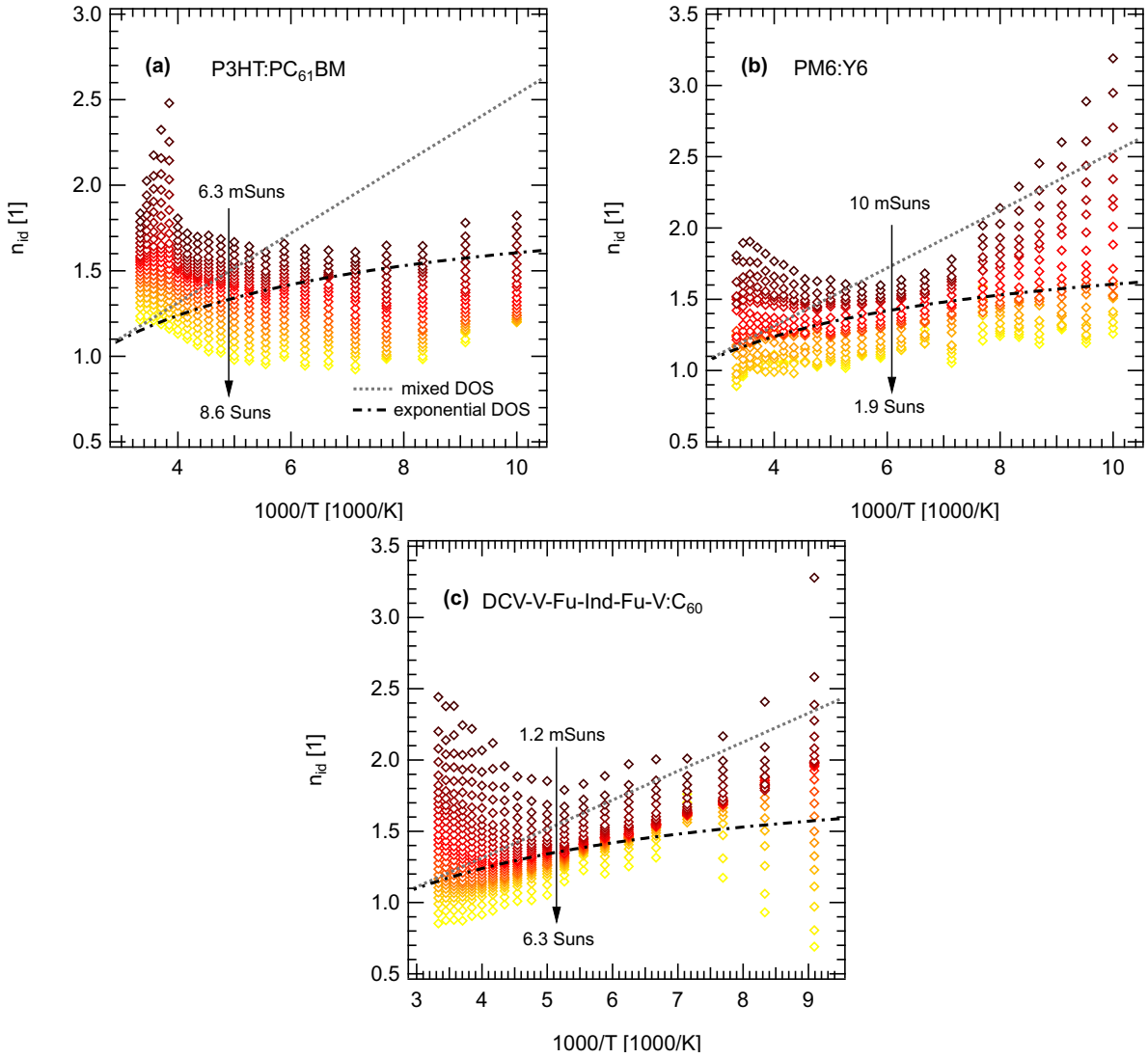


**Figure S05.** Light intensity-dependent ideality factors of (a) P3HT:$PC_{61}$BM, (b) PM6:Y6 and (c) DCV-V-Fu-Ind-Fu-V:$C_{60}$ as a function of the inverse temperature. At higher illumination intensities the ideality factor decreases below unity due to surface recombination.[19] At lower light intensities low shunt resistance leads to unphysically high values of the ideality factor. The ideality factors for mixed and exponential DOS models (dashed lines) are calculated according to Eqs. (3) and (4) in the main text, respectively, using $E_U = 35$ meV.

**Open-circuit voltage-resolved ideality factors**. Supposing that the density of states differs from the exponential, the slope of the distribution $E_U$ depends on the energetic position in the DOS. An exponential is acting as a local approximation of the real DOS at a given energy. Hence, the ideality factor depends additionally on the temperature dependence of the QFLS, and has to be resolved energetically. Figure S06 shows the difference between the light intensity and the open-circuit voltage–resolved ideality factors.

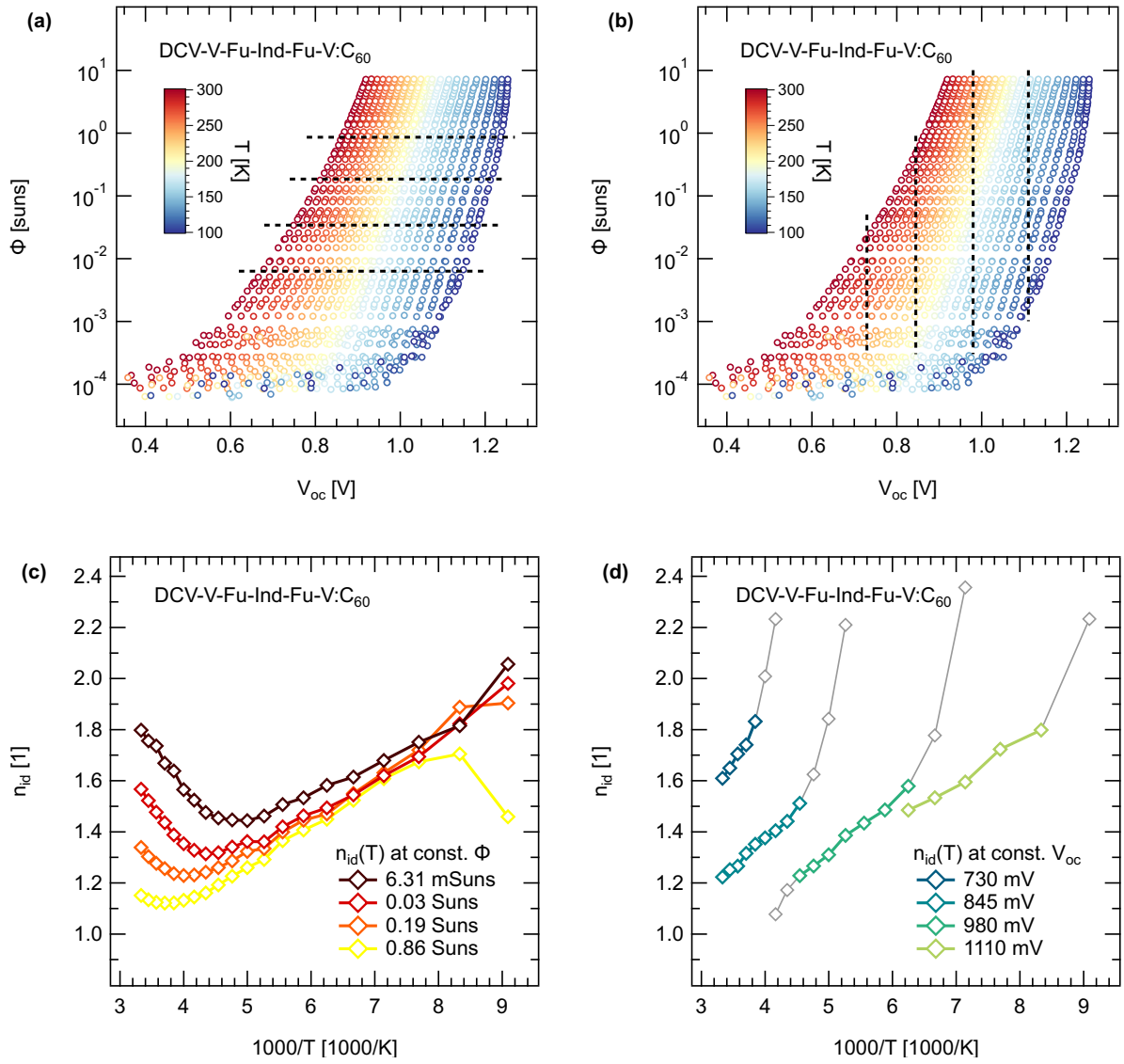


**Figure S06.** Temperature dependent Suns–$V_{oc}$ data of DCV-V-Fu-Ind-Fu-V:$C_{60}$ (a) labelling few values of illumination intensity and (b) open-circuit voltage. (c) Light intensity-dependent ideality factors $n_{id}(\Phi, T)$ corresponding to the dashed lines in (a). (d) Open-circuit voltage-resolved ideality factors $n_{id}(V_{oc}, T)$ corresponding to the dashed lines in (b). The values of $n_{id}$ exceeding 2.4 are omitted. The ideality factors affected by surface recombination and low shunt resistance are indicated by grey colour, and are excluded from Figure 2 in the main text.

**The Urbach energy**. The Urbach energy $E_U$ is calculated from $n_{\mathrm{id}}$ using Eq. (3) for mixed DOS, and Eq. (4) for exponential DOS models. In Figure S07 the values not affected by low shunt resistance and surface recombination (coloured circles) converge at different temperatures, leading to temperature-independent Urbach energy. Leakage currents and surface recombination cause substantial deviation of $E_U$ (grey circles) from the common trend. These unphysical values of the Urbach energy are excluded from Figure (3) in the main text.

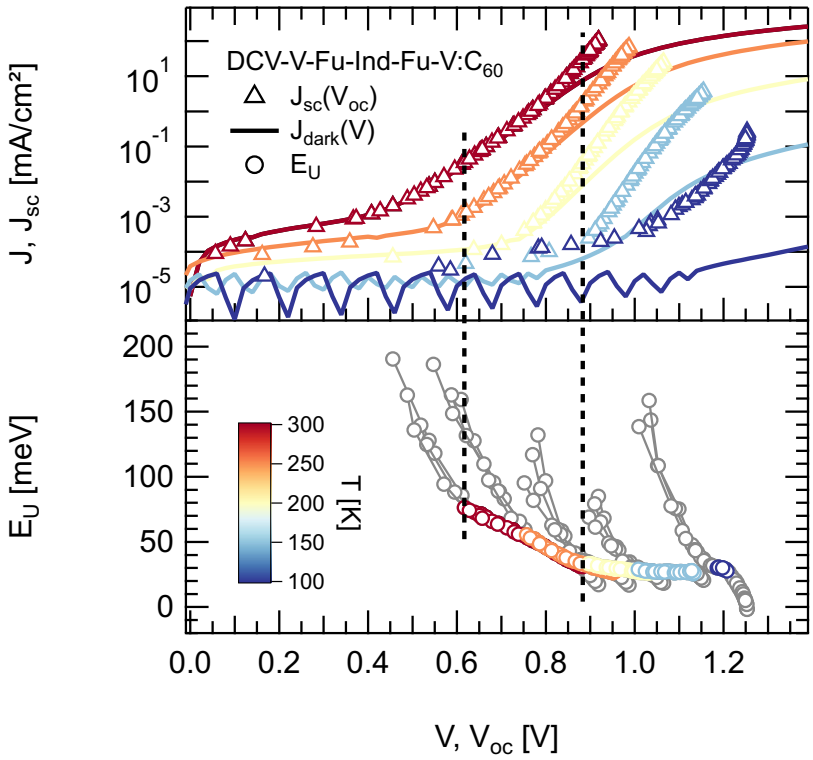


**Figure S07.** (Top) $J_{\mathrm{sc}}\,(V_{\mathrm{oc}})$ of DCV-V-Fu-Ind-Fu-V:$C_{60}$ at selected temperatures are compared to dark $J\,(V)$ to show the influence of shunt on the Suns-$V_{\mathrm{oc}}$ data. (Bottom) Corresponding $E_U$ converge at different temperatures (coloured). Surface recombination ($n_{\mathrm{id}} < 1$) and leakage currents cause $E_U$ divergence from the coloured values (grey).[19]


[1] R. Fitzner, E. Mena-Osteritz, A. Mishra, G. Schulz, E. Reinold, M. Weil, C. Körner, H. Ziehlke, C. Elschner, K. Leo, M. Riede, M. Pfeiffer, C. Uhrich, and P. Bäuerle, Journal of the American Chemical Society **134**, 11064 (2012).
[2] P. Mark and W. Helfrich, Journal of Applied Physics **33**, 205 (1962).
[3] J. C. Blakesley and D. Neher, Physical Review B **84**, 075210 (2011).
[4] T. Kirchartz and J. Nelson, Physical Review B **86**, 165201 (2012).
[5] A. Hofacker and D. Neher, Physical Review B **96**, 245204 (2017).
[6] B. Xiao, P. Calado, R. C. MacKenzie, T. Kirchartz, J. Yan, and J. Nelson, Physical Review Applied **14**, 024034 (2020).
[7] V. Arkhipov, V. Kolesnikov, and A. Rudenko, Journal of Physics D: Applied Physics **17**, 1241 (1984).
[8] G. Paasch and S. Scheinert, Journal of Applied Physics **107**, 104501 (2010).
[9] S. Baranovskii, Physica Status Solidi (b) **251**, 487 (2014).
[10] T. Kirchartz, B. E. Pieters, J. Kirkpatrick, U. Rau, and J. Nelson, Physical Review B **83**, 115209 (2011).
[11] I. Lange, J. Kniepert, P. Pingel, I. Dumsch, S. Allard, S. Janietz, U. Scherf, and D. Neher, The Journal of Physical Chemistry Letters **4**, 3865 (2013).
[12] S. D. Collins, C. M. Proctor, N. A. Ran, and T.-Q. Nguyen, Advanced Energy Materials **6**, 1501721 (2016).
[13] G. Garcia-Belmonte, Solar Energy Materials and Solar Cells **94**, 2166 (2010).
[14] T. M. Burke, S. Sweetnam, K. Vandewal, and M. D. McGehee, Advanced Energy Materials **5**, 1500123 (2015).
[15] R. A. Street, A. Krakaris, and S. R. Cowan, Advanced Functional Materials **22**, 4608 (2012).
[16] A. Foertig, J. Rauh, V. Dyakonov, and C. Deibel, Physical Review B **86**, 115302 (2012).

[17] K. Tvingstedt and C. Deibel, Advanced Energy Materials **6**, 1502230 (2016).
[18] L. Perdigón-Toro, L. Q. Phuong, F. Eller, G. Freychet, E. Saglamkaya, J. I. Khan, Q. Wei, S. Zeiske, D. Kroh, S. Wedler, A. Köhler, A. Armin, F. Laquai, E. M. Herzig, Y. Zou, S. Shoaee, and D. Neher, Advanced Energy Materials **12**, 2103422 (2022).
[19] T. Kirchartz, F. Deledalle, P. S. Tuladhar, J. R. Durrant, and J. Nelson, The Journal of Physical Chemistry Letters **4**, 2371 (2013).